A NOVEL ANTIMATTER DETECTOR BASED ON X-RAY DEEXCITATION OF EXOTIC ATOMS

KAYA MORI,[1] CHARLES J. HAILEY,[1] EDWARD A. BALTZ,[1] WILLIAM W. CRAIG,[2] MARC KAMIONKOWSKI,[3]
WILLIAM T. SERBER,[1] AND PIERO ULLIO[4]

ABSTRACT

We propose a novel antiparticle detector. The gaseous antiparticle spectrometer (GAPS) effects particle identification through the characteristic X-rays emitted by antiparticles when they form exotic atoms in gases. GAPS obtains particularly high grasp (effective area–solid angle product) at lower particle energies, where conventional schemes are most limited in their utility. The concept is simple and lightweight, so it can be readily employed on balloon- and space-based missions. An extremely powerful potential application of GAPS is a space-based search for the neutralino through the detection of a neutralino annihilation by-product—the antideuteron. Paradoxically, this space-based search for the neutralino is capable of achieving comparable sensitivity to as yet unrealized third-generation, underground dark matter experiments. And GAPS can obtain this performance in a very modest satellite experiment. GAPS can also provide superior performance in searches for primary antiprotons produced via neutralino annihilation and black hole evaporation and in probing subdominant contributions to the antiproton flux at low energies. In a deep space mission, GAPS will obtain higher sensitivity for a given weight and power than BGO calorimeters.

Subject headings: atomic processes — cosmic rays — dark matter — techniques: spectroscopic

1. INTRODUCTION

The gaseous antiparticle spectrometer (GAPS) identifies antiparticles through the characteristic X-rays emitted by antimatter when it forms exotic atoms in gases. GAPS provides an order of magnitude or more improvement in sensitivity compared to conventional magnetic spectrometers at substantially lower weight and cost. GAPS is thus ideal for space-based experiments. In § 2 of the paper we describe the scientific opportunities that can be exploited with the superior sensitivity of GAPS. We particularly focus on a high-sensitivity, indirect search for the neutralino through detection of cosmic antideuterons. This approach to neutralino detection can yield sensitivities comparable to or even exceeding those of as yet unrealized third-generation, underground dark matter experiments. We also discuss more prosaic possibilities, such as measurement of the very low energy antiproton spectrum. We also mention more exotic possibilities, such as searching for antiprotons from evaporating black holes and searching for antihelium with much greater sensitivities than the AMS experiment on the *International Space Station* (*ISS*). In § 2 we describe the basic GAPS concept, in § 3 the atomic physics of exotic atoms, in § 4 the detector efficiency, in § 5 issues of background rejection, and in § 6 results of preliminary simulation.

1.1. *Indirect Detection of Dark Matter through Antideuterons*

A major goal of twenty-first-century physics is to identify particle dark matter. The best candidate is likely a weakly interacting massive particle (WIMP; Jungman, Kamionk-owski, & Griest 1996) such as those that arise from supersymmetric extensions of the standard model of particle physics. Most effort has concentrated on the neutralino, the lightest supersymmetric partner. The neutralino can be detected by the nuclear recoils it produces through its scalar and vector couplings to matter. Major direct detection experiments are underway, but they are extremely difficult because of the low predicted count rate for the neutralino. These experiments must be done deep underground to shield against cosmic rays and, in particular, neutrons produced in the atmosphere and through muon interactions (the tertiary neutrons). Tertiary neutrons, as well as those produced in (α, n)-reactions in the surrounding rock, are particularly problematic for these direct detection experiments. The experiments cannot distinguish a target atom recoil due to a neutron from one due to a neutralino. Therefore, Monte Carlo simulations are required to estimate neutron contribution to the nuclear recoil. The recent controversy over the possible detection of the neutralino by DAMA and the contradictory claims of the CDMS experiment hinge on the reliability of the neutron background estimation (Akerib 2001).[5] This situation requires considerable caution, and it has been advocated that a reliable neutralino detection may require several experiments operating with different target nuclei and obtaining consistent neutralino detection rates. Ideally, such experiments would have different intrinsic background sources. However, all underground direct detection experiments have neutrons as the dominant source of uncertainty.

Alternately, many indirect detection schemes have been proposed for the neutralino (Gondolo 2001).[6] These rely on the fact that the neutralino is a Majorana particle and thus can annihilate with itself. The resultant heavy quarks and gauge and Higgs bosons produce hadronic and electromagnetic showers. This leads to a primary antiproton com-

[1] Columbia Astrophysics Laboratory, 538 West 120th Street, New York, NY 10027.

[2] Lawrence Livermore National Laboratory, 7000 East Avenue, Livermore, CA 94550.

[3] California Institute of Technology, Mail Code 130-33, Pasadena, CA 91125.

[4] SISSA, via Beirut 4, S4014 Trieste, Italy.

[5] See http://nu2000.sno.laurentian.ca/D.Akerib.

[6] See http://nu2000.sno.laurentian.ca/P. Gondolo.

ponent to the cosmic rays. The antiproton component has been discussed in many papers and searched for in many experiments. It is difficult to distinguish the primary antiproton component from the secondary component produced in cosmic-ray interactions in the interstellar medium (§ 1.2 below). Both line and continuum γ-ray signatures have been proposed as a means to search for the neutralino with *GLAST*. In addition, it has been proposed to search for the neutrino signature produced when neutralinos annihilate in the gravitational potential well of the Sun (Andrés et al. 1999).

The promise of indirect detection techniques to search for the neutralino has changed markedly in the last year. Theoretical calculations predict a flux of primary antideuterons in the cosmic rays due to the annihilation of the neutralino (Donato, Fornengo, & Salati 2000). Like the well-known primary antiproton signal, the antideuteron signal is produced when WIMPs annihilate to heavy quarks and gauge and Higgs bosons that fragment to cosmic-ray antiprotons and antineutrons. This flux is large enough that the GAPS technique, when employed in a modest space-based experiment, has competitive and possibly superior sensitivity to as yet unrealized third-generation direct detection experiments. Indeed, the indirect detection of the neutralino via the antideuteron provides an ideal complementary technique to the direct detection experiments because its background source is not neutrons (see below).

Figure 1 shows the projected sensitivity of CDMS II, a state-of-the-art direct detection experiment, through the year 2004. Also shown is the projected sensitivity of GENIUS, a proposed third-generation experiment based

on ∼1 ton germanium. The third-generation experiments will improve on the second-generation experiments by about 3 orders of magnitude. The dots represent the ensemble of SUSY models parameterized by their spin-independent cross section and neutralino mass. A similar plot is shown in Figure 2 for a modest MIDEX class satellite experiment (described in more detail in § 6.1). The sensitivity calculation is all inclusive (including the effects of orbit-varying geomagnetic cutoff and solar modulation). The sensitivity for this (unoptimized) experiment is much more than an order of magnitude better than AMS for detecting the antideuteron. Recently a $g-2$ experiment has detected a marginal (2.7 σ) discrepancy in the anomalous magnetic moment for the muon (Brown et al. 2001). If this discrepancy is due to supersymmetric corrections to loop diagrams producing the magnetic moment, then the range of possible SUSY models is severely constrained, as shown by the green circles in Figures 1 and 2 (Baltz & Gondolo 2001). Unlike the AMS experiment on *ISS*, the GAPS experiment on a small satellite can be as sensitive as a third-generation experiment and will access nearly the entire allowed SUSY parameter space as restricted by the $g-2$ results.

The source of background in a primary antideuteron search is the secondary antideuterons produced in cosmic-ray interactions. The situation is reminiscent of the primary antiproton searches, where the background is due to secondary and tertiary antiprotons (Simon, Molnar, & Roesler 1998; Bergström, Edsjö, & Ullio 1999). However, the situation is much better for a primary antideuteron search. The secondary antideuterons cut off at much higher kinetic
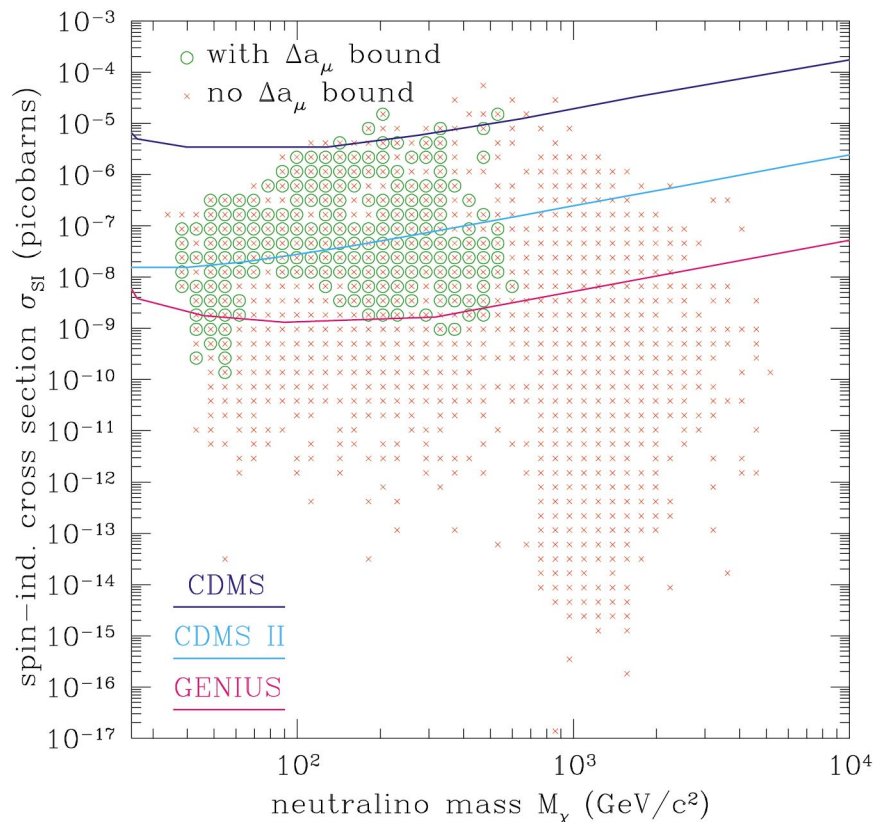

Fig. 1.—Sensitivity of current/planned underground experiments for neutralino detection for various SUSY models (Bergström & Gondolo 1996; Edsjö & Gondolo 1997; Edsjö 1997; Bergström, Edsjö, & Gondolo 1998; Baltz & Edsjö 1999; Mandic, Baltz, & Gondolo 2001). The green circled SUSY models are those allowed if the anomalous muon $g-2$ result is correct (Baltz & Gondolo 2001).
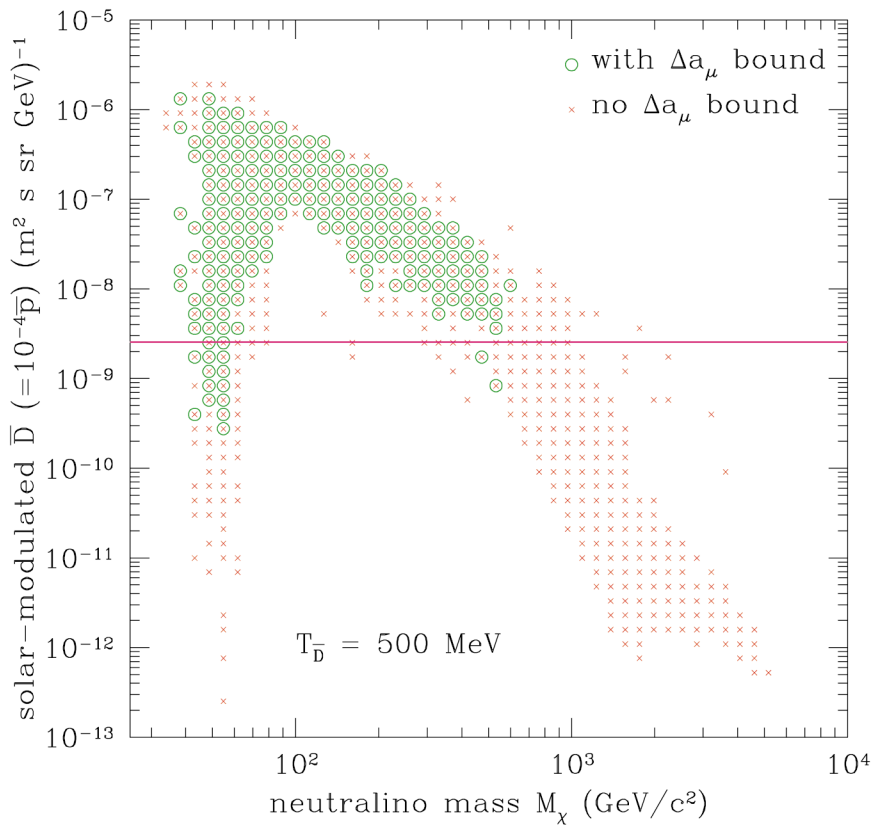
Fig. 2.—Sensitivity of a MIDEX class GAPS implementation for neutralino detection shown with the same set of models as in Fig. 1. The antideuteron flux is obtained by rescaling the solar-modulated antiproton flux of Bergström et al. (1999) by a factor 10^{-4} (Donato et al. 2000).

energy than in the case of secondary and tertiary anti-protons (Fig. 3). If primary antideuterons are searched for at low enough energies, the probability of contamination by secondary antideuterons can be made negligible, in contra-distinction to the primary antiproton case.

The antideuteron search provides a nice complement to the direct detection experiments seeking the neutralino. With their very different sources of background, they can together provide a convincing case for the neutralino detec-tion. In addition, there are WIMP models in which the antideuteron signal would be present but a measurable signal in a direct detection experiment would not be obtained.

1.2. Spectroscopy of Ultralow Energy Antiprotons

The antiproton spectrum has been the subject of numer-ous theoretical and observational papers. This is a vast subject, and we restrict our comments to those areas where GAPS represents a significant improvement over current techniques and where the discovery space is substantial. An example is the use of GAPS on an interstellar probe to characterize the ultralow energy antiproton spectrum. At comparable mass, volume, and power consumption, GAPS has almost an order of magnitude more grasp ($A\Omega$ product) than alternatives, can probe to lower antiproton energies, and can do so with superior discriminatory power against false detections (§ 6.2).

The secondary antiprotons are produced through $p + p \rightarrow \bar{p} + X$ reactions, and the kinematic suppression of the secondary antiprotons due to the requirement of three protons in the final state, combined with the decreasing

primary proton spectrum, provides a very characteristic shape for the secondary antiproton spectrum. This has been probed in many balloon flights and will be measured by AMS on *ISS*. The very sharp suppression of the secondary
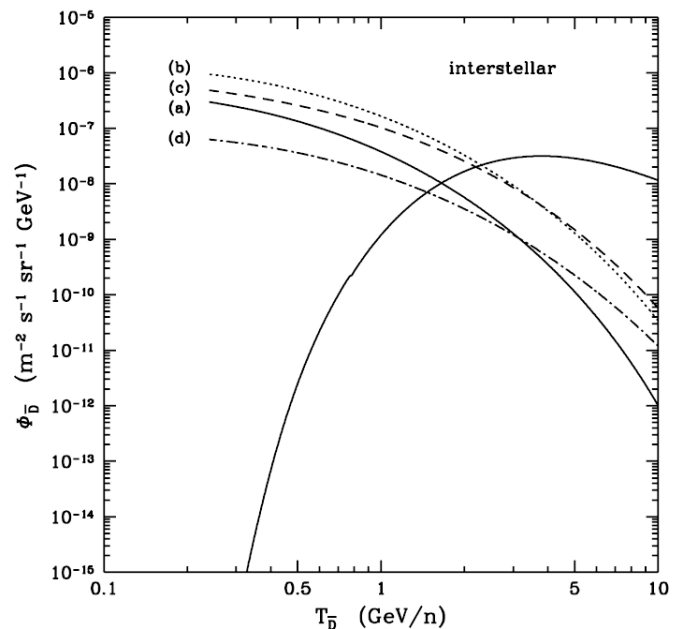

Fig. 3.—Interstellar flux of secondary antideuterons (*heavier solid curve*) decreases at low energy, whereas the energy spectrum of the anti-deuterons from supersymmetric origin (*curves a–d*) tends to flatten (from Donato et al. 2000).
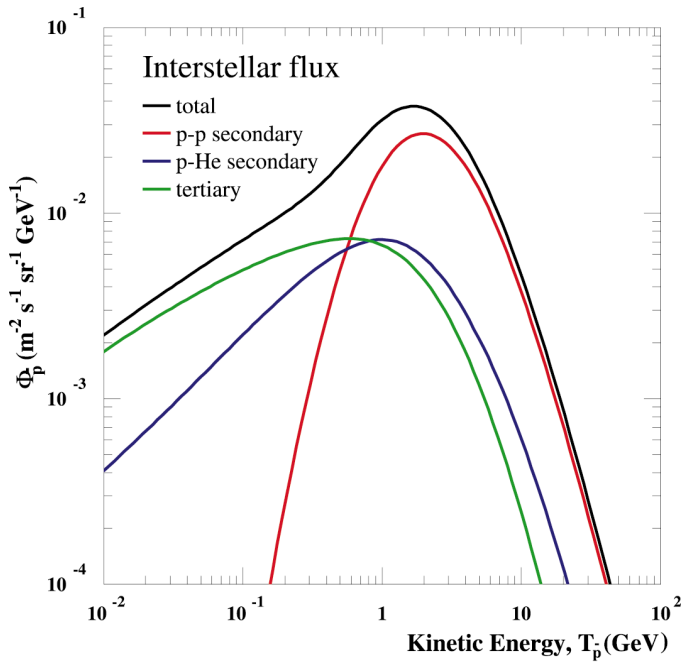
Fig. 4.—Cosmic-ray–induced interstellar antiproton flux

antiproton flux at low energies provides an opportunity to test subdominant contributions to the antiproton flux (Simon et al. 1998; Bergström et al. 1999; Donato et al. 2001). These processes include collisions of primary protons with heavier nuclei (mainly helium) and energy losses of the secondary antiprotons during propagation (producing the tertiary antiprotons component). These separate components are shown in Figure 4. The effect of these subdominant components is marked below ~ 150 MeV. But the ability to probe these components is limited by the effects of solar modulation and the geomagnetic rigidity cutoff inherent in low Earth orbit missions. The modulation prevents antiprotons with energies of less than order the solar potential (~ 500 MeV) from reaching the vicinity of the Earth. In order to surmount this difficulty, it has been proposed to send a probe out of the heliosphere (Wells, Moiseev, & Ormes 1999). In § 6.2, we show how a 1 yr observation with GAPS on such a probe can detect secondary and tertiary antiprotons down to 40 MeV.

Several sources of primary antiprotons could be even larger than the secondary and tertiary antiproton signal. Antiprotons are produced in the neutralino annihilation and dominate over the secondary and tertiary components below ~ 100 MeV for some SUSY models (Jungman & Kamionkowski 1994; Bottino et al. 1998). The evaporation of primordial black holes can produce a signal below 100 MeV, which is much larger than either the neutralino-induced antiproton signal or the secondary or tertiary signals, yet can still evade detection on either balloon experiments or AMS, which operates at much higher energies (MacGibbon & Carr 1991; Maki, Mitsui, & Orito 1996).

1.3. Antihelium

The discovery of a single antihelium atom is compelling evidence for the existence of an antimatter domain in the universe. Such searches are highly problematic and thus difficult to motivate. In particular, observational con-

straints require such domains to be large enough that the antihelium must travel over great distances through the intergalactic magnetic field and penetrate into our own galaxy against the galactic wind. There is substantial uncertainty in the losses that would occur because of these effects (Streitmatter 1996). Moreover, inflationary cosmologies may provide additional theoretical biases against the promise of such searches. Recent attempts to suggest the possibility of a local source of antihelium that has evaded previous observational limits seem strained (Belotsky et al. 2000). Nevertheless, the GAPS approach, when implemented as a means to search for the antideuterons, can provide a 2 order of magnitude improvement in sensitivity over AMS in setting bounds on the $\bar{\mathrm{He}}/\mathrm{He}$ ratio.

2. THE GAPS CONCEPT

Antimatter spectrometers must identify particle type and energy. Detection schemes for all proposed and forthcoming missions can be classified in two categories: magnetic spectrometers and calorimeters. Magnetic spectrometers measure particle rigidity from which momentum and charge-to-mass ratio can be determined. Calorimeters identify antiparticles by searching for events with a total energy deposit equal to twice the rest energy of the antiparticle, as is obtained from an antiparticle slowed down in the calorimeter and captured/annihilated by a nucleus. In both schemes the velocity is measured by the time-of-flight (TOF) method, which is also used to reconstruct the incident energy.

Magnetic spectrometers have an increasing error in rigidity/momentum identification below 200 MeV nucleon^{-1} because of multiple scattering, which results in an inaccurate determination of deflection angle. Also, the effective solid angle for particle acceptance tends to be small for a given spectrometer surface area since an incident particle has to enter the magnetic field in a certain angular range for efficient deflection. Calorimeters also have drawbacks as antiparticle detectors. For instance, in identifying antiprotons, the calorimeter searches for events whose energy deposit is twice the proton rest energy. But normal hadronic interactions in the calorimeter initiated by protons, the most common particle incident on the calorimeter, can produce an energy deposit identical to the antiproton. Therefore, the TOF must be used to exclude those incoming protons whose total kinetic energy is $2m_p c^2$. The requirement to use the TOF to reject particle velocities corresponding to this energy, and in the face of enormous proton fluxes, is challenging. Indeed, it requires far better TOF discrimination than has previously been obtained. Moreover, the calorimeter has the disadvantage that the antiproton signature is not unique—it is simply indicative of a certain energy deposit. Both the magnetic spectrometer and the calorimeter tend to be heavy for a given grasp, in the former case because of the magnets and the latter case because of the need to have a thick enough crystal to completely contain the antiparticle annihilation γ-rays.

A GAPS detector configuration consisting of a single channel (for illustrative purposes) is shown in Figure 5. An antiparticle that passes through a TOF system (which measures energy) is slowed down by dE/dx loss in a degrader block. The thickness of this block is tuned to select the sensitive energy range of the detector. The antiparticle is stopped in the gas chamber, forming an exotic atom with probability of order unity. The exotic atom is in a high
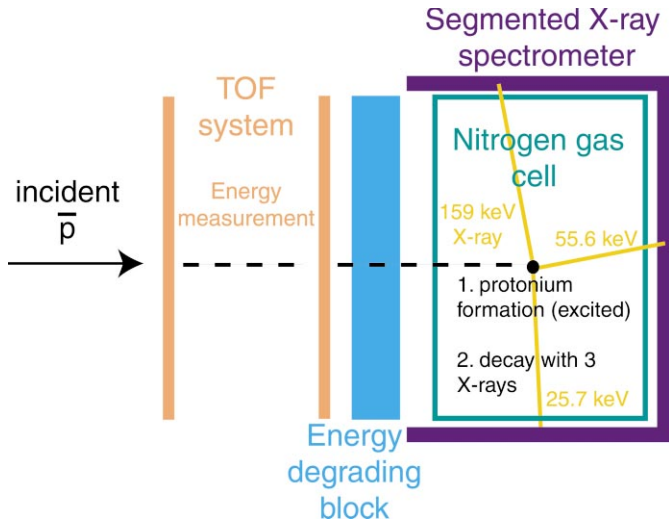
Fig. 5.—Operating principal of the GAPS detector using antiprotons as an example.

excitation state, which deexcites through a process involving both autoionizing transitions and radiation-producing transitions. Through proper selection of the target gas and its pressure, the absorption of the antiparticle can be tailored to produce three to four well-defined X-ray transitions in the exotic atom decay chain. Promptly after the release of these X-rays, the antiparticle annihilates in the nucleus, producing a shower of pions.

The X-rays have energies in the 25-250 keV range, so the gas and the surrounding gas chamber support structure are optically thin to them. These X-rays are absorbed in a CZT or NaI spectrometer that surrounds the gas cell. The coincident signals between the TOF system, the characteristic decay X-rays, and the energy deposition of the pions provide a clean, positive confirmation of the detection of an antiparticle. The energy of the X-rays uniquely define the antiparticle mass.

The above design is only illustrative. A realistic design (§ 6) contains more than 10 gas cells, each surrounded by a segmented X-ray detector and the entire structure surrounded by the TOF. This configuration provides substantial stopping power so that antiparticles can be stopped over a broad energy band through the narrowband stopping power of each cell. Moreover, this segmented design allows for optically thin gas cells (so that the ladder X-rays can reach the X-ray detector), but permits very high pressure in the small individual cells. In this manner, GAPS can achieve high X-ray detection efficiency along with total energy bandwidths ~ 0.5 GeV nucleon^{-1}.

This technique of antiparticle identification and background rejection provides a number of advantages, particularly for the detection of low-energy ($E < 1$ GeV nucleon^{-1}) antiparticles. These include extremely high grasp, low weight per grasp, and extremely low probability of false particle identification. In addition, there is no inherent lower limit on the detectable antiparticle energy. Instead, it is set by the geomagnetic rigidity and the energy losses in materials (e.g., the TOF) outside the target gas.

The GAPS concept depends on the detection of the deexcitation X-rays in gas targets. The definitive experiments were done in noble gases by Bacher et al. (1988). A detailed understanding of the relevant atomic physics is necessary to apply these results to the optimization of GAPS. We discuss the relevant issues in the next section.

3. ATOMIC PROCESSES IN EXOTIC ATOMS

3.1. Fate of a Captured Antiparticle in Exotic Atoms

Once an antiparticle $\bar{X}$ is slowed down to an energy of order the ionization energy of the atom, the antiparticle is captured into an exotic atom replacing a bound electron. The cross section for trapping of $\bar{X}$ is of the order of a molecular cross section (Beck, Wilets, & Alberg 1993). The captured antiparticle is in a highly excited state, $n_0 = (M^*/m_e)^{1/2}$ (assuming that $\bar{X}$ replaces a K-shell electron), because of energy conservation (Hayano et al. 1994). For instance, $n_0 \sim 40$ for an antiproton. M^* is the reduced mass of the $\bar{X}$-atom system. $\bar{X}$ decays via a radiative transition or an Auger process. A radiative transition emits a photon from the exotic atom, while the Auger process ionizes a bound electron. The Auger process sets in when the transition energy of $\bar{X}$ exceeds the ionization energy of bound electrons. Usually, the Auger process is fast compared to the radiative transitions. Since larger changes in Δn and $\Delta l = \pm 1$ are preferred for the deexcitation (dipole selection rule), $\bar{X}$ will drop to the so-called circular state in which the orbital angular momentum takes its largest value by the transition $(n, l) \rightarrow (n' = n - 1, l' = n - 2)$. Although the Auger process may lead $\bar{X}$ to other than the circular states with small branching ratio (Hartmann 1990), $\bar{X}$ will be in a circular state at an early stage in its decaying process. Decay of circular states proceeds by $\Delta n = -1$, $\Delta l = -1$ due to the selection rules for ladder transitions. A simplified version of the decay process is

(1) capture of an antiparticle into an initial bound state (n_0, l_0),
(2) decay of the antiparticle into a circular state $(n, n - 1)$,
(3) deexcitation via radiative or Auger ionization of L- and M-shell electrons,
(4) complete depletion of bound electrons,
(5) radiative decay of the antiparticle with emission of characteristic X-ray, and
(6) annihilation of the antiparticle in the nucleus with a pionic shower.

In order to identify an incident antiparticle, we measure photons from the radiative ladder transitions after all the bound electrons are ionized. Atomic calculation is simplified for the electron-depleted exotic atoms, since it reduces to a two-body problem of the antiparticle and the nucleus. Our concern is concentrated mainly on transition energy, lifetime of the exotic atom, and quantum number of complete ionization.

3.1.1. Ladder Transition Energy

The photon energy in ladder transition $n \rightarrow n - 1$ is given by

$$E_{\text{ladder}}(n) = \tilde{Z}^2(\eta M^*)\left[\frac{1}{(n - 1)^2} - \frac{1}{n^2}\right] \text{ ryd}, \quad (1)$$

where M^* is the reduced mass of $\bar{X}$ in units of proton mass m_p and $\eta = m_p/m_e$. The terms z and Z are the charge of the incident particle and the absorbing atom, and we define $\tilde{Z} = zZ$ for convenience. Ladder transition energies are listed in Tables 1–3.

TABLE 1

LADDER TRANSITION ENERGIES (keV) FOR THE ANTIPROTON

Transition	$Z = 7$	$Z = 8$	$Z = 10$	$Z = 18$
$2 \to 1$	857.7	1130.	1787.	5927.
$3 \to 2$	158.8	209.2	330.9	1097.
$4 \to 3$	**55.59**	**73.22**	**115.8**	384.2
$5 \to 4$	**25.73**	**33.89**	**53.60**	177.8
$6 \to 5$	13.98	18.41	**29.12**	**96.60**
$7 \to 6$	8.427	11.10	17.56	**58.25**
$8 \to 7$	5.470	7.204	11.40	37.81
$9 \to 8$	3.750	4.939	7.813	25.92

NOTE.—Numbers in boldface are energies of the candidate photons observable by GAPS.

3.1.2. Lifetime of an Antiparticle in the Exotic Atom

The transition rate, $\Gamma_{\text{ladder}}(n)$ (s^{-1}), for ladder transition ($n \to n - 1$) is given by

$$\Gamma_{\text{ladder}}(n) = \frac{4 E_{\text{ladder}}(n)^3}{3 \hbar^4 c^3} |\langle n-1, n-2 | r | n, n-1 \rangle|^2$$

$$= 5.9 \times 10^{13} M^* \tilde{Z}^4 n^{-5} . \qquad (2)$$

Therefore, the transition time is

$$\tau_{\text{ladder}}(n) \sim 1.6 \times 10^{-14} M^{*-1} \tilde{Z}^{-4} n^5 \text{ s.} \qquad (3)$$

When $\bar{X}$ replaces an electron in shell N_{sh} ($N_{\text{sh}} = 1, 2,$ and 3 corresponds to K-, L-, and M-shell, respectively), its initial bound state is $n_0 \sim N_{\text{sh}} (\eta M^*)^{1/2}$. The lifetime $\tau_{\bar{X}}$ is given by

$$\tau_{\bar{X}} \sim 10^{-5} N_{\text{sh}}^6 M^{*2} \tilde{Z}^{-4} \text{ s.} \qquad (4)$$

This is an upper limit to the lifetime that assumes that all the transitions are via radiative deexcitation. Delay of the annihilation of antiprotons in helium was observed by Nakamura et al. (1994), indicating the formation of antiprotonic helium atoms with lifetime of order 10^{-6} s.

3.1.3. Principal Quantum Number of Complete Ionization

When the transition energy of $\bar{X}$ becomes larger than the K-shell ionization energy of a bound electron, the Auger process ionizes a K electron. The quantum number n_K where electrons are completely depleted is given by

$$E_{\text{ladder}}(n_K) = I_K (= Z^2 \text{ ryd}) . \qquad (5)$$

In this case, n_K is independent of Z. The number n_K is ~ 15, 19, and 38 for $\bar{p}$, $\bar{D}$, and $\bar{He}$, respectively. Bacher et al. (1988) observed strong suppression of $n = 15, 16$ ladder X-rays in several noble gases illuminated by antiproton beams. All the transitions from $n < n_K$ are radiative, and ladder photons from lower n (e.g., $n = 4$–7 for $\bar{p}$) are observed by X-ray detectors.

TABLE 2

LADDER TRANSITION ENERGIES (keV) FOR THE ANTIDEUTERON

Transition	$Z = 7$	$Z = 8$	$Z = 10$	$Z = 18$
$3 \to 2$	297.8	395.1	632.0	2143.
$4 \to 3$	**104.2**	**138.3**	221.2	750.1
$5 \to 4$	**48.24**	**64.01**	102.4	347.2
$6 \to 5$	**26.21**	**34.77**	55.61	188.6
$7 \to 6$	15.80	20.97	**33.53**	**113.7**
$8 \to 7$	10.26	13.61	21.76	**73.81**
$9 \to 8$	7.031	9.330	14.92	**50.60**
$10 \to 9$	5.030	6.673	10.67	36.20
$11 \to 10$	3.721	4.938	7.897	26.78

TABLE 3

LADDER TRANSITION ENERGIES (keV) FOR ANTIHELIUM

Transition	$Z = 7$	$Z = 8$	$Z = 10$	$Z = 18$
$6 \to 5$	186.4	250.4	408.1	1440.
$7 \to 6$	**112.4**	151.0	246.1	868.4
$8 \to 7$	**72.93**	**97.98**	159.7	563.6
$9 \to 8$	**50.00**	**67.17**	**109.5**	386.4
$10 \to 9$	**35.77**	**48.05**	**78.32**	276.4
$11 \to 10$	26.46	**35.55**	**57.95**	204.5
$12 \to 11$	20.13	27.04	**44.07**	155.5
$13 \to 12$	15.66	21.04	34.30	**121.0**
$14 \to 13$	12.42	16.70	27.22	**96.04**
$15 \to 14$	10.03	13.47	21.96	**77.48**
$16 \to 15$	8.206	11.02	17.97	**63.41**

3.2. Relevant Atomic Processes and Their Transition Rates

In order to increase efficiency for detecting $\bar{X}$, high-density targets are desirable for the detection medium. As the density increases, several atomic processes may interfere with the identification of characteristic X-rays from the ladder transitions. Figure 6 schematically shows the deexcitation path of an exotic atom, and Figure 7 presents the rates of different atomic transitions discussed in the following section.

3.2.1. Stark Mixing

A quantum state of $\bar{X}$ becomes degenerate after the full ionization of bound electrons. Then the electric field from an adjacent atom, $E = (e/R^3) R$, distorts different l quantum states, inducing $\Delta n = 0$ transitions. R is the intermolecular distance or impact parameter of a passing atom in the gas. This transition leads $\bar{X}$ to an S-state followed by a nuclear annihilation or to an $nS \to 1S$ radiative transition. The photon energy from the $nS \to 1S$ radiative transition in high-Z materials is too high to be measured by a thin X-ray detector. A measure of the transition width caused by the energy shift $\Delta E_{\text{Stark}} = \langle n, n-2 | e E \cdot r | n, n-1 \rangle$ is (Day,
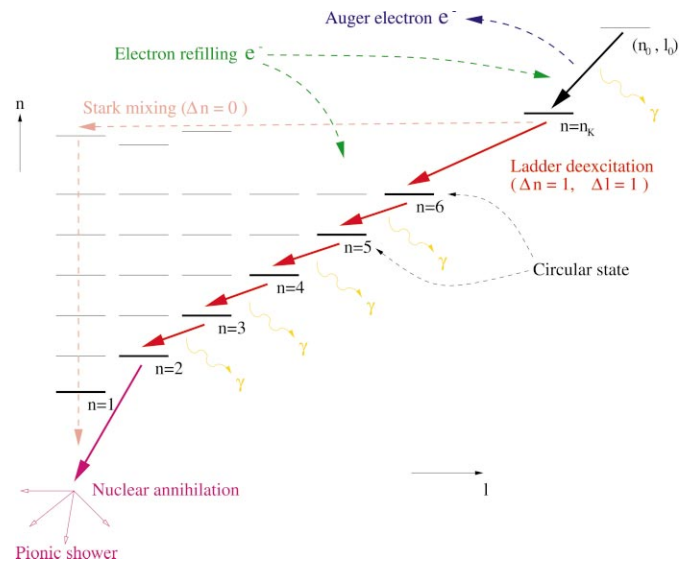
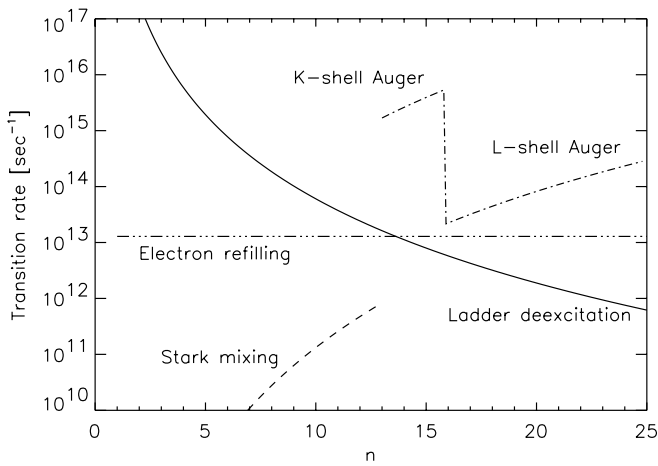FIG. 6.—Deexcitation path of a captured antiparticle in an exotic atom

FIG. 7.—Competing atomic processes in antiprotonic argon atom at $\rho = 0.5$ g cm^{-3}, $T = 0°$ C, and $\sigma_r = 10^{-14}$ cm^2. All the bound electrons are ionized at $n_K = 13$ because of the delay of complete ionization by electron refilling. The rate of Auger ionization was calculated by Ferrell's formula (Ferrell 1960).

Snow, & Sucher 1959)

$$\omega_{\text{Stark}}(R) \sim \frac{\Delta E_{\text{Stark}}}{\hbar} = 2.2 \times 10^{13} M^{*-1} R^{-2} \tilde{Z}^{-1} n^2 \ . \quad (6)$$

Stark mixing becomes dominant over the ladder transition when $R \leq R_n$, where R_n (in units of Bohr radius a_0) is given by

$$\omega_{\text{Stark}}(R_n) \sim \Gamma_{\text{ladder}}(n) \quad (7)$$

or

$$R_n \sim 0.6 M^{*-1} \tilde{Z}^{-5/2} n^{7/2} \ . \quad (8)$$

R_n can be larger than the intermolecular distance in a solid or a liquid. This leads to suppression of the ladder X-ray transitions of interest. However, molecules in a gas follow the Boltzmann distribution and present different impact parameters to the exotic atom. For this collisional process, the rate of Stark mixing is given by

$$\Gamma_{\text{Stark}} = N_a (\pi R_n^2) v \ . \quad (9)$$

N_a is the number density of atoms. We represent the velocity of atoms v in the gas by their thermal velocity $v_{\text{th}} = (3kT/Am_p)^{1/2}$, where A is the atomic weight of the gas. Therefore,

$$\Gamma_{\text{Stark}}(n) = 3.1 \times 10^{12} M^{*-2} \tilde{Z}^{-5} A^{-3/2} n^7 \rho T^{1/2} \ , \quad (10)$$

where ρ and T are the density (g cm^{-3}) and temperature (K) of the gas.

3.2.2. Electron Refilling

When an exotic atom is highly ionized, charge transfer from other neutral atoms can refill shells in the exotic atom. Charge transfer may cause a continual cycle of Auger ionization at rates high enough to suppress the radiative transitions. The cross section for charge transfer from adjacent atoms is in the range of $\sigma_r = 10^{-14}$–10^{-15} cm^2 (Ryufuku, Sasaki, & Watanabe 1980). When n_e is the number density of electrons and $\sigma_{r,-14}$ is the cross section of electron refilling in units of 10^{-14} cm^2, the rate of electron refilling is given by

$$\Gamma_{\text{refill}} = n_e \sigma_r v_{\text{th}} = 4.7 \times 10^{13} A^{-1/2} \rho T^{1/2} \sigma_{r,-14} \ . \quad (11)$$

Metals are not appropriate target materials because their fast Fermi velocities ($\sim 10^8$ cm s^{-1}) lead to rapid refilling rates.

3.2.3. Nuclear Absorption

The strong nuclear decay rate of the $2P$-state in protonium is $\Gamma_{2P} = 35$ meV (Reifenröther & Klempt 1989), corresponding to $\Gamma_{2P} = 5.3 \times 10^{13}$ s^{-1}. Nuclear annihilation for the $2P$-state can be as fast as its radiative deexcitation. The $2 \to 1$ ladder transition is also excluded from observable line candidates since its transition energy is much higher than the energy band of a moderately thick X-ray detector. The strong interaction in D-states is negligible (Reifenröther & Klempt 1989).

3.3. Yield of Ladder Transitions

The initial capture angular momentum l_0 is not well understood presently. However, we can assume a statistical distribution for l_0; i.e., a probability for the capture of an antiparticle into states l_0 is given by $(2l_0 + 1)/n_0^2$. An antiproton captured into $l_0 = 0$–5 is not relevant, since it decays into a low-n circular state that does not give several ladder transition photons observable by a thin X-ray detector. However, the probability of capture into such a low-l_0 state is less than 10%. Coulomb deexcitation, a process by which transition energy is transferred to kinetic energy of the exotic atom and a nearby atom, reduces the yield of ladder transition photons (Aschenauer et al. 1995). However, the significance of the Coulomb deexcitation is still not well understood and is likely a small effect.

In experiments it has been shown that the yield of ladder transitions is dependent on the gas pressure. The yield of ladder transitions ($n \geq 7$) was measured to be $\sim 50\%$ for relatively low pressure ($\sim 10^{-2}$ atm) gases forming antiprotonic atoms (Bacher et al. 1988). On the other hand, Lyman lines were measured at high gas pressures (≤ 170 atm) for muonic atoms (Jacot-Guillarmod et al. 1988). Hereafter, we set the yield of the overall ladder transitions $Y_{n_1} = 50\%$ (n_1 is the first circular state of the ladder transitions of interest) and $Y_n = 100\%$ ($n < n_1$; lower n ladder transitions). We will investigate the pressure dependence of the yield of ladder transitions at antiproton beaming facilities.

3.4. Optimal Gas Element and Density

Atomic calculation sets an upper limit on the acceptable gas density required to generate the characteristic X-rays from the ladder transitions. At high density, Stark mixing and electron refilling can suppress the radiative deexcitations. However, Stark mixing does not set in when electrons are present in the exotic atom, and so the electron refilling can suppress the Stark mixing as well. Therefore, the optimal situation is for the ladder transition rate to be faster than the Stark mixing rate by the time electrons no longer refill the exotic atom (more precisely, refill the K-shell). Refilling of the L-shell can still be faster than ladder transitions. However, at $n \leq 7$, the fluorescence transitions of L-shell electrons to the K-shell become slower than the ladder transition in antiprotonic atoms. This condition is explicitly described as

$$\Gamma_{\text{ladder}}(n_K) > \max \{\Gamma_{\text{Stark}}, \Gamma_{\text{refill}}\} \ . \quad (12)$$

Therefore,

$$\rho(\text{g cm}^{-3}) < \min \left\{ 1.9 \times 10^1 M^{*3} \tilde{Z}^9 A^{3/2} n_K^{-12} T^{-1/2} \, , \right.$$

$$\left. 1.3 M^* \tilde{Z}^4 A^{1/2} n_K^{-5} T^{-1/2} \sigma_{r,-14}^{-1} \right\} . \tag{13}$$

We plot the maximum density for several gases in Figure 8. Hydrogen and helium are ruled out because of their fast Stark mixing rate at the gas density desirable for stopping antiparticles. On the other hand, Kr and Xe are not optimal because of high photoabsorption of ladder X-rays observable with X-ray detectors. Therefore, we limit our choice of the gas to N_2, O_2, Ne, and Ar. Gas selection will be discussed further in the following sections.

4. DETECTION EFFICIENCY

We assume a cubic detector for a preliminary calculation of detection efficiency. A detailed description of the detector design will be found in § 5. Hereafter, we denote the kinetic energy of an incident particle as $E_{\bar{X}}$, its incident direction as $\hat{n} = (\theta, \phi)$, and an incident point on the detector surface S as $r = (x, y, z)$. The total detection efficiency is the product of the efficiency of forming an exotic atom in the gas (ϵ_{cap}) and detecting ladder X-rays (ϵ_γ):

$$\epsilon_{\text{tot}}(E_{\bar{X}}, \hat{n}, r) = \epsilon_{\text{cap}} \epsilon_\gamma . \tag{14}$$

The term ϵ_γ is decoupled from ϵ_{cap} since it depends only on the photon energies and the point C at which $\bar{X}$ is captured. Effective grasp $A\Omega(E_{\bar{X}})$ (m^2 sr) is given by

$$A\Omega(E_{\bar{X}}) = \int d\Omega \int dS \, \epsilon_{\text{tot}}(E_{\bar{X}}, \hat{n}, r) . \tag{15}$$

We define an energy band by integrating $A\Omega(E_{\bar{X}})$ over energy and dividing by the peak $A\Omega(E_{\bar{X}})$.

4.1. Efficiency of Forming an Exotic Atom

The quantum efficiency of forming an exotic atom in the gas is given as

$$\epsilon_{\text{cap}} = \epsilon_{\text{cap}}(E_{\bar{X}}, \hat{n}, r) = P_{\text{cap}}(1 - P_{\text{ann}})\epsilon_{\text{rig}} . \tag{16}$$

A capture point C is uniquely determined for a given set of parameters ($E_{\bar{X}}, \hat{n}, r$). P_{cap} is defined as the probability of capturing antiparticles in the gas obtained by subtracting

the capture fraction in the X-ray detector. Since the cross section of the antiparticle capture is rather insensitive to Z (Cohen 2000), we simply assume that P_{cap} is the ratio of the gas column density to the total column density in the detector. P_{ann} is a probability of the direct annihilation with the nucleus (§ 4.1.2). The term ϵ_{rig} represents the effect of the geomagnetic rigidity cutoff (§ 4.1.3).

4.1.1. Stopping Power and Range of Antiparticles

We adopt data for stopping power and range from the NIST PSTAR database (Berger, Coursey, & Zucker 1999). Data from PSTAR are applicable to antiprotons in the so-called Bethe-Bloch regime ($E_p > 10$ MeV). For $\bar{D}$ and $\bar{He}$, we used a well-known scaling law (Leo & Haase 1994).

At low energy ($E_{\bar{p}} < 10$ MeV), there are several minor effects that can cause ranges for antiprotons to deviate from the proton data. The difference in the sign of charge affects the stopping power below 1 MeV (Barkas, Dyer, & Heckman 1963). The stopping power for antiprotons becomes roughly twice as large as protons at the Bloch peak (~ 1 MeV; Adamo et al. 1993). The estimated deviation in range is about 1% for $E_{\bar{p}} = 10$ MeV. Multiple scattering by atomic electrons modifies the direction of incident particles (significant at $E_{\bar{p}} < 1$ MeV). Hence, effective range will be shorter than the mean range assuming a straight-line projectile. Because of its heavy mass compared to an electron, the estimated error is less than 1% for a 10 MeV antiproton (Berger et al. 1999). The statistical distribution in range, so-called range straggling, must be taken into account. A parameter $\kappa = \bar{\Delta}/W_{\text{max}}$, where $\bar{\Delta}$ is the mean energy loss and W_{max} is the maximum energy transfer in a single collision, is much larger than 1 for the typical detector configuration. This implies that the range straggling is well described by a Gaussian distribution in the thick absorber approximation (Leo & Haase 1994):

$$f(x, \Delta) = \exp \left[\frac{-(\Delta - \bar{\Delta})^2}{2\sigma^2} \right] , \tag{17}$$

where

$$\sigma^2 = 0.1569 \frac{Z}{A} \rho x \, (\text{MeV}^2) . \tag{18}$$

The term x is the distance over which a particle propagates in a material with density ρ. For a material with thickness 1
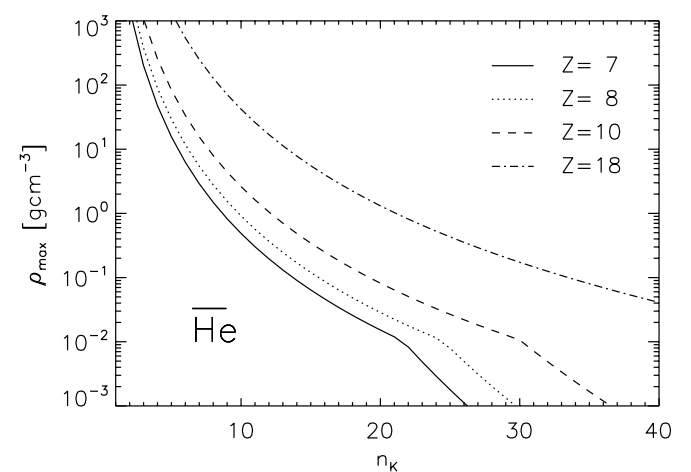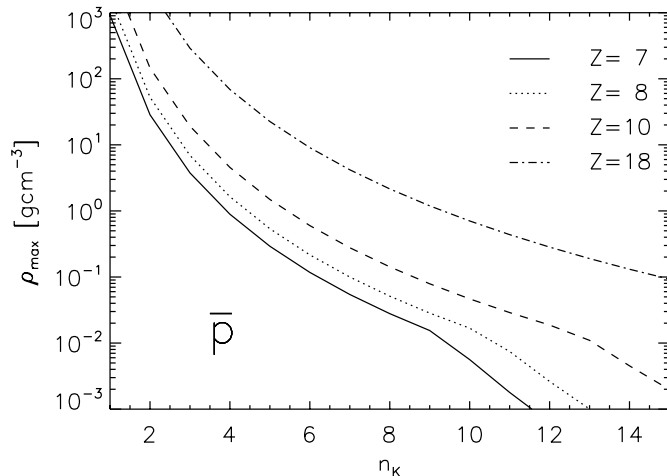

FIG. 8.—Maximum gas density ρ_{max} (g cm^{-3}) for antiprotons (*left panel*) and antihelium (*right panel*). The temperature is $T = 0°C$ for illustrative purposes.

g cm^{-2} and 50 MeV antiprotons, the estimated error is less than 1%.

4.1.2. *Probability of the Direct $\bar{X}$ Annihilation with the Nucleus*

Cross sections for direct annihilation of antiprotons have recently been studied. The lowest energy experiment was done at $E_{\bar{p}} = 1$–20 MeV by the OBELIX collaboration (Bertin et al. 1996). Another experiment by Brückner et al. (1990) provided data at $E_{\bar{p}} = 20$–200 MeV. Although a $1/v$ law is valid at high energies, this is modified by Coulomb attraction between the antiparticle and the nucleus at low energy. A general form for the annihilation cross section is (Kurki-Suonio & Sihvola 2000)

$$\sigma_{\mathrm{ann}} = \sigma_0 \, C(v^*, \tilde{Z})/v^* \, , \tag{19}$$

where

$$C(v^*, \tilde{Z}) = \frac{2\pi \tilde{Z} \alpha c/v^*}{1 - \exp(-2\pi \tilde{Z} \alpha c/v^*)} \, . \tag{20}$$

The term v^* is the velocity of an incident particle in the center of mass frame. We fitted the above formula to the experimental data, obtaining $\sigma_0 = 12.7$ mbarn. The probability of direct annihilation when $\bar{X}$ is decelerated from $E_{\bar{X}} = E_0$ to E_1 is given by

$$P_{\mathrm{ann}} = 1 - e^{-\tau_{\mathrm{ann}}} \, , \tag{21}$$

$$\tau_{\mathrm{ann}} = \int_{E_0}^{E_1} N_a \, \sigma_{\mathrm{ann}}(E) \left(\frac{dE}{dx}\right)^{-1} dE \, . \tag{22}$$

Since the stopping power is almost independent of the material type, τ_{ann} is insensitive to the atomic number Z. Loss of antiparticles by direct annihilation is 5%–10% in the typical configuration of GAPS.

4.1.3. *Geomagnetic Rigidity*

The efficiency of particle detection depends on the orientation of the detector and particles with respect to the geomagnetic field. The minimum rigidity at some geomagnetic latitude ϱ and geocentric radius R is given by

$$R_{\mathrm{min}} = \frac{\mu_{\oplus}}{R^2} \frac{\cos^4 \varrho}{[(1 + \cos \theta \cos^3 \varrho)^{1/2} + 1]^2} \, , \tag{23}$$

where $\mu_{\oplus}$ is the Earth's dipole moment and $\mu_{\oplus}/R_{\oplus}^2 = 60$ GV (Zombeck 1982; Donato et al. 2000). The term θ is the angle between the direction of arrival of the particle and the tangent to the circle of latitude. For a given orbit, we computed $\epsilon_{\mathrm{rig}}(E_{\bar{X}}, \Omega_{\mathrm{det}})$ as a fraction of the observation time in which a particle of kinetic energy less than $E_{\bar{X}}$ can reach the detector within its viewing angle Ω_{det}. For instance, assuming the detector sees the entire sky, $\epsilon_{\mathrm{rig}}(E_{\bar{D}} = 1 \text{ GeV}$ nucleon$^{-1}) = 0.2$ on the *ISS* orbit (52° north), while it is increased to 0.4 at 70° north, where a high-latitude space mission is possible.

4.2. *Quantum Efficiency of Photon Detection*

The quantum efficiency for detecting exotic atom photons γ_i with energy E_{γ_i} at a point C is given by

$$\epsilon_{\gamma}(C) = \prod_i \epsilon_{\gamma_i}(E_{\gamma_i}, C) \, , \tag{24}$$

$$\epsilon_{\gamma_i}(E_{\gamma_i}, C) = Y_{n_i} e^{-\tau_{\gamma_i}} \epsilon_{\mathrm{det}}(E_{\gamma_i}) \, . \tag{25}$$

Y_{n_i} is the yield of ladder transition $n_i \rightarrow n_i - 1$; τ_{γ_i} is the optical depth of a photon γ_i in the gas and the pressure

vessel; and $\epsilon_{\mathrm{det}}(E_{\gamma_i})$ is the quantum efficiency of the photon detector.

We adopt data for photo attenuation lengths (g^{-1} cm^2) from the NIST database (Hubbell & Seltzer 1997). We simply assume the attenuation of photons in the photon detector is $\epsilon_{\mathrm{det}}(E_{\gamma_i})$. We take angle-averaged values for ϵ_{γ_i} since the direction in which a photon is emitted from the exotic atom is random.

5. DETECTOR DESIGN

The effective grasp and the bandwidth depend mainly (or only) on the target gas column density. High column density provides a larger acceptance. On the other hand, the gas column density is limited by the photoattenuation. In order to overcome this intrinsic difficulty, we have designed a cubic detector of dimension L (m) segmented into numerous cells. A cell of size l (m) consists of gas surrounded by a X-ray detector (Fig. 9). While the overall gas column density is large, photons emitted from an exotic atom travel only short distance to reach the X-ray detectors surrounding the cell.

A gas column density of 1 g cm^{-2} is selected so that the observable X-rays do not undergo serious photoabsorption or Compton scattering in the gas. We need to sustain a gas pressure as high as ~ 50 atm in the gas chamber. By use of low-Z high-strength material (e.g., carbon fiber, reinforced plastic), photoattenuation in the pressure vessel wall is negligible. On the other hand, optimization of the thickness of the X-ray detectors is more complicated. The X-ray detector must be thick enough to absorb the ladder X-rays but thin enough to result in negligible absorption of antiparticles. Compromise between these two factors results in the X-ray detector column density about 1 g cm^{-2}. Outside the X-ray detector lattice, we locate two plastic scintillators of the total thickness 1 cm separated by 25 cm for the velocity measurement with a time resolution ~ 50 μs.

5.1. *Energy Band*

The outermost X-ray detector and the plastic scintillators are sufficiently thin for 50 MeV nucleon^{-1} antiparticles to penetrate. With degraders for slowing down high-energy particles, we can have at most five energy channels corresponding to each surface of the cubic detector except the bottom. While the column density of the gas and the X-ray detector of a cell is fixed to ~ 1 g cm^{-2}, the size of the cells as well as the gas density is determined for different configurations by taking into account other constraints, such as the maximum weight (or size) allowed for a given mission. The typical value for the total column density is 5–10 g cm^{-2}, corresponding to a bandwidth of 50–70 MeV nucleon^{-1} in each channel.

5.2. *Background*

Detection of antiparticles requires extremely reliable identification in the presence of enormous particle backgrounds. The antiproton flux is $\sim 10^5$ times lower than the proton flux, while ~ 1 antideuteron might be observed for every $\sim 10^9$ protons and $\sim 10^5$ deuterons. There are several kinds of "background." For instance, a cosmic-ray–produced antideuteron can be mistaken for a neutralino-produced antideuteron. This is not really a misidentification of the antiparticle but rather its production mechanism. The backgrounds in this section are those that cause an antiparticle to be misidentified as another particle or anti-
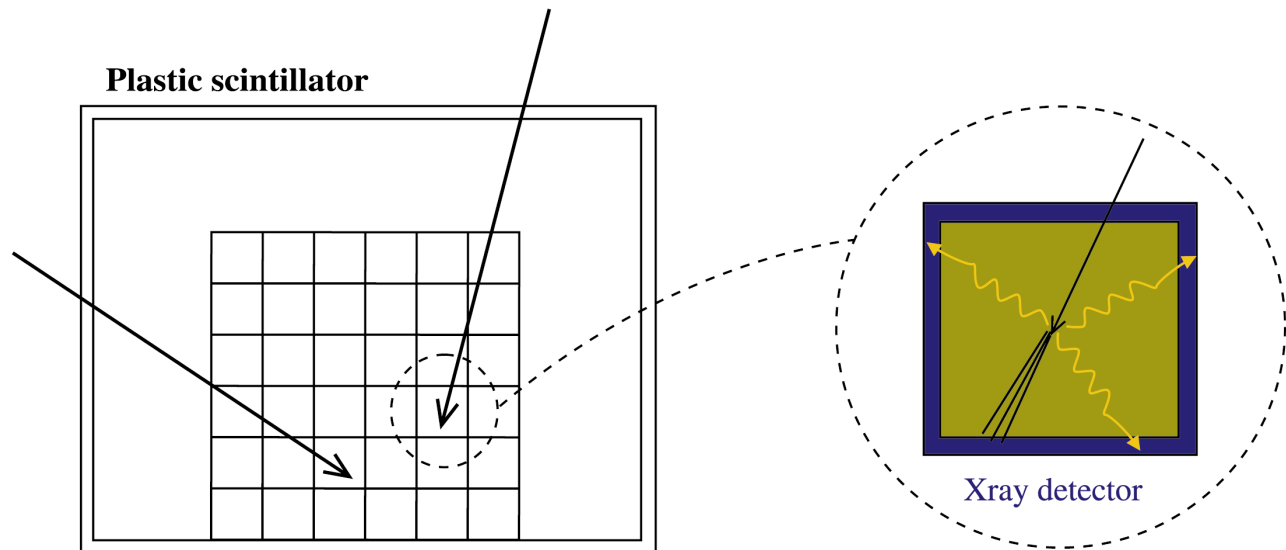
Plastic scintillator

Xray detector

Fig. 9.—Schematic view of the detector consisting of numerous cubic cells. Each cell is a gas chamber surrounded by a pressure vessel and X-ray detectors.

particle. This background is a set of X-rays whose energies exactly mimic the antiparticle ladder X-rays and that occur in a time window when a candidate event has triggered the TOF. For instance, a proton may produce a TOF signal in the energy band of interest while activation of the detector volume by cosmic rays leads to the emission of three or more X-rays or even β-particles mimicking the X-rays of protonium during the time the TOF trigger occurs. This would lead to the misidentification of the proton as an antiproton. Similar considerations apply to the antideuteron. The background X-rays can also be produced by hadronic or pionic interactions leading to radiation, such as bremsstrahlung, or even a direct ionization energy deposit of the same magnitude as that produced by a ladder X-ray transition.

The proper consideration of background is complicated and the subject of ongoing study. We mention only some of the key issues here. GAPS should ideally operate at high latitudes to enhance the flux of antiparticles. But that also means very high proton fluxes. The γ-ray and β-particle background from spallation and activation by cosmic rays must be estimated. In addition, the pionic showers produced during annihilation of an antiparticle are a source of secondary X-rays, which can confuse the identification of one antiparticle for another or serve as a source of background, leading to a misidentification of a particle in an adjacent detection cell. Much more work is required to understand the sources of background and their exact impact. However, we have attempted to estimate the background for the most aggressive use of GAPS: an antideuteron experiment in a highly inclined orbit (§ 6.1). We used data from the balloon experiment GRATIS (Keck et al. 2001) to scale to the satellite experiment using procedures well described in the literature (Harrison et al. 2001). The typical background for this orbit of $\sim$10 counts cm^{-2} s^{-1} in the relevant energy band of the ladder transitions is almost 2 orders of magnitude higher than in an experiment at the midlatitudes because of effects of increased particle flux on activation, spallation, and secondary γ-ray background in the payload. This background estimation indeed includes all the potential sources because it is

based on measured X-ray background in previous space and balloon experiments. We have extrapolated background rates at higher latitude orbit by estimating increase of cosmic-ray rate based on geomagnetic rigidity, which is found in § 4.1.3. For the energy resolution of the CZT and a 10 μs time resolution, the probability of detecting three photons in the right energy and time window to mimic an antiproton for the $\sim$ 1 m^2 area of the design below is $\sim$8 $\times$ 10^{-9}. This is sufficient to ensure negligible misidentification of protons as antiprotons.

The same calculation can be done for antideuterons. Here, there is a significant effect since protons, which are the dominant source of misidentifications, can be rejected with modest efficiency by the TOF because their energy deposit differs from that of an antideuteron. This is sufficient to reach the $\sim$10^{-12}–10^{-14} rate of accidental misidentification per proton, which is required. Other sources of background leading to misidentifications are less important than those considered here. We have probably underestimated the true rejection power. Much of the background that we considered is generated when activation γ-rays of higher energy than the ladder transition X-rays Compton scatter in a detection cell, leading to a partial energy deposit mimicking a ladder transition X-ray. The scattered γ-ray will be absorbed in another cell, allowing a possibility of using other detection cells as part of a veto system for such events. Pionic X-rays are also produced in the nuclear annihilation and when used in coincidence with ladder X-rays can provide additional discriminatory capability. We have not yet investigated their potential.

We should also note that GAPS has no problem distinguishing antiprotons from antideuterons because the ladder transition X-rays are uniquely identified in the two cases. This scheme is dramatically different than the approach of Wells et al. (1999). It does not require any calorimetric signature for identification. The fact that the relevant X-ray signature is "constrained" in one detection cell provides additional flexibility for rejecting background that needs to be investigated.

We primarily envision GAPS being employed with high energy resolution CZT detectors. However, alkali halide

scintillator crystals such as NaI(Tl) provide a simpler and cheaper alternative X-ray detector. The background rejection capability of NaI(Tl) is comparable or even somewhat better than CZT. The poorer energy resolution is more than offset by the superior temporal resolution compared to CZT. If NaI is used, the energy resolution is sufficient so that the antiproton and antideuteron can be resolved cleanly through the comparison of the highest energy of the three ladder X-rays of interest in each case (refer to Tables 1 and 2). The two lowest energy X-rays from the antiprotonic and antideuteronic atoms cannot be resolved from each other in NaI. The preference for CZT is primarily based on the belief (to be studied) that it will be easier to implement the highly segmented readout system and multicell detection geometry. In addition, the accuracy to which the three to four ladder X-rays can be measured in CZT provides a very powerful positive confirmation of the presence of antimatter.

6. POTENTIAL APPLICATION OF THE GAPS DETECTOR

We discuss a few potential applications of GAPS based on model calculation of instrument performance.

6.1. Antideuteron

As discussed in § 1.1, a sensitivity $\sim 10^{-9}$ m^{-2} sr^{-1} GeV^{-1} s^{-1} is required below 1 GeV nucleon^{-1}. A multi-year space mission is required to achieve such sensitivities. We have simulated a high inclination (70° north) mission. The high-latitude mission (HLM) is advantageous in reducing the geomagnetic rigidity cutoff. Assuming nitrogen gas and 27 GAPS cells of size $l = 160$ cm surrounded by pixilated CZT detectors, we achieve a peak grasp of 9.0 m^2 sr for antideuterium over an energy band of 0.1–0.4 GeV nucleon^{-1} with the detector size of $L = 5$ m and a total mass of less than 10,000 pounds (Table 4). This results in the sensitivity 2.6×10^{-9} m^{-2} sr^{-1} GeV^{-1} s^{-1} in 3 yr, 20 times better than AMS (Table 5). A model calculation of the effective grasp for the proposed experiment is in Figure 10. In addition to superior sensitivity to AMS, we also note that the cost of a GAPS instrument with 20 times the sensitivity of AMS is about an order of magnitude less. The type of mission described here could readily be executed as a modestly sized NASA MIDEX class mission.

6.2. Antiproton

The recent BESS measurements detected only a few antiprotons below 200 MeV, with resultant large error bars. To

TABLE 4

CONFIGURATION OF THE HIGH-LATITUDE MISSION FOR DETECTION OF THE ANTIDEUTERON AND ANTIHELIUM

Parameter	Value
Latitude	70° north
Total size L (m)	5
Weight (ton)	≤ 5
Overall column density (g cm^{-2})	5
Number of cells	27
Gas element	Nitrogen
Peak effective grasp (m^2 sr) for $\bar{D}$ ($\overline{He}$)......	9.0 (11.1)
Energy band (GeV nucleon^{-1})	0.1–0.4

NOTES.—The peak effective grasps are for the lowest energy channel. Bandpasses of other channels are shifted to high energy by the degrader.

TABLE 5

COMPARISON OF THE SENSITIVITY OF PRIMARY ANTIDEUTERON DETECTION

Observation	$I_{\bar{D}}$ (m^{-2} sr^{-1} GeV^{-1} s^{-1})	Energy Band (GeV nucleon^{-1})
GAPS on HLM......	2.6×10^{-9}	0.1–0.4
AMS on *ISS*[a].........	4.8×10^{-8}	0.1–2.7

NOTE.—Observation time is 3 yr.
[a] Solar minimum. It is 3.2×10^{-8} at solar maximum.

detect a statistically significant number of antiprotons in several low-energy bands at $E_{\bar{p}} < 0.5$ GeV requires a sensitivity of $\sim 10^{-3}$ m^{-2} sr^{-1} GeV^{-1} s^{-1}. We simulated a balloon-borne experiment performed at high latitude where the rigidity cutoff is less than 0.5 GeV. The detector size is $L = 2$ m, and the overall detector column density is 9 g cm^{-2}. It consists of $5 \times 5 \times 5 = 125$ cubic cells of size $l = 40$ cm. The estimated total weight of the detector is less than 4000 pounds. Neon gas is chosen since three ladder X-rays (29.12, 53.60, and 115.8 keV) are observable by a 1 g cm^{-2} thick NaI detector (preferred over CZT on a balloon experiment because it is cheaper). The effective grasp is 2.4 m^2 sr with a bandwidth ~ 70 MeV for each energy channel. This is 4–8 times larger than the geometrical grasp of the AMS and BESS experiments, respectively. Acceptance for each energy channel is 1.4×10^4 m^2 sr GeV s for a 1 day observation time. In several balloon flights over the 11 yr solar cycle, one could study the effect of solar modulation or any excess from the predicted secondary flux at five different energy bands over $E_{\bar{p}} = 120$–400 MeV.

The most effective means of probing exotic sources of antiprotons, such as the evaporation of primordial black holes (MacGibbon & Carr 1991; Maki et al. 1996) or the annihilation of neutralinos (Jungman & Kamionkowski 1994; Bottino et al. 1998), is to send an instrument into deep space beyond the heliosphere. An instrument in deep space is far removed from solar modulation effects and geomagnetic rigidity cutoff inherent in low Earth orbit missions. This permits investigation of low-energy antiprotons, especially at $E_{\bar{p}} < 100$ MeV. We have designed a detector with two energy channels. A measurement in the lower energy
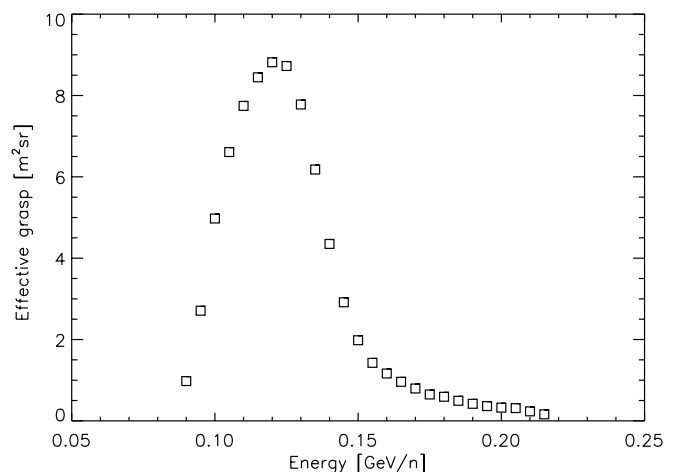

FIG. 10.—Effective grasp (m^2 sr) for the detection of the antideuteron. The detector configurations for high-latitude mission are presented in Table 5. This is for the lowest energy channel. The sharp cutoff at low energy is due to the particle degradation by the outermost CZT detector and the plastic scintillators.

TABLE 6

Estimated Number of Antiprotons Measured by 1 Year
Interplanetary Probe

Source	40–60 MeV	100–120 MeV
Secondary (no p-p)	20	30
Neutralino annihilation	60	100
Primordial black hole evaporation......	280	400

Note.—The effective grasp is 65 cm^2 sr for each channel.

band 40–60 MeV, where the flux due to p-p interactions is negligible, is to obtain a clean signature of the p + He and tertiary antiprotons or these in combination with a possible neutralino signature and/or primordial black hole signature. The second channel at 100–120 MeV anchors the antiproton flux and spectral shape to higher energy observations.

The detector is a cubic cell of size $L = 6$ cm comparable with a recently proposed BGO detector by Wells et al. (1999). Argon gas is mandatory from the constraint on the gas density discussed in § 3.4. All six surfaces of the cube see the whole sky, and they are divided into two energy channels by properly mounting degraders. The effective grasp is 65 cm^2 sr for each channel, 6 times larger than the geometrical grasp of the BGO detector, while the estimated weight of the detector is a few kilograms, less than the BGO detector. In addition, the background rejection power of GAPS is far better. In Table 6, we estimate the overall counts from the intensities for interstellar antiprotons. GAPS is able to constrain a source of antiprotons by a 1 yr observation.

6.3. Antihelium

Previous measurements set an upper limit on the ratio $\bar{He}$/He of 10^{-6} (Saeki et al. 1998; Battiston 1998b). The AMS/ISS experiment will be able to set upper limits of $\bar{He}$/He of 10^{-9} with 95% confidence (Battiston 1998a). In Figure 11, we present the sensitivities of $\bar{He}$ detection for our satellite-based antideuteron search. We obtained a sensitivity of $\sim 1.5 \times 10^{-9}$ m^{-2} sr^{-1} GeV^{-1} s^{-1}. This translates to a $\bar{He}$/He of $\sim 3.8 \times 10^{-11}$ with 95% confidence, assuming the He flux in the GAPS energy band is 1.6×10^{2} m^{-2} sr^{-1} $(GeV\ nucleon^{-1})^{-1}$ s^{-1}. Our limit is ~ 100 times better than the AMS/ISS mission. Our increased sensitivity to the $\bar{He}$/He ratio is partly due to operating at lower energies where the He flux is more copious and partly due to greatly increased grasp over AMS. There are (potential) complications in interpreting
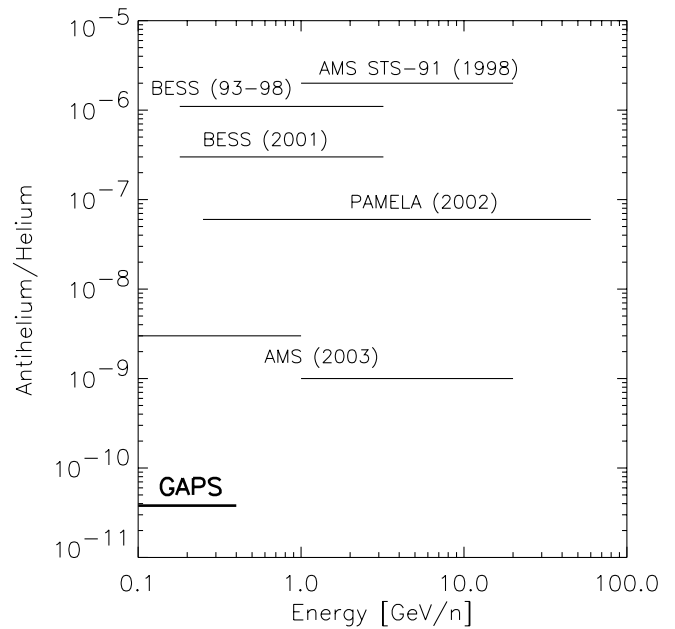

Fig. 11.—Comparison of the upper limits of the ratio $\bar{He}$/He

the "real" improvement in sensitivity versus AMS because the leakage of $\bar{He}$ into our galaxy is energy dependent because of galactic wind and magnetic field effects (Streitmatter 1996). However, given the uncertainties in the theory, it is not meaningful at this time to try to correct for such effects.

7. SUMMARY

We have presented a novel scheme for detecting antimatter that has high sensitivity, especially at lower energies where conventional techniques are inefficient. It also provides an unambiguous signal for the presence of antimatter. Current effort will focus on development of more accurate models of background in the GAPS detector and development of effective strategies for using the available information from the detector matrix to reject this background. Ultimately a prototype will be built and tested.

REFERENCES

Adamo, A., et al. 1993, Phys. Rev. A, 47, 4517
Akerib, D. 2001, in Neutrino 2000: Proceedings of the XIXth International Conference on Neutrino Physics and Astrophysics, ed. J. Law, R. W. Ollerhead, & J. J. Simpson (New York: Elsevier)
Andrés, E. C., et al. 1999, Nucl. Phys. B (Proc. Suppl.), 77, 474
Aschenauer, E. C., et al. 1995, Phys. Rev. A, 51, 1965
Bacher, R., Blüm, P., Gotta, D., Heitlinger, K., Schneider, M., Missimer, J., Simons, L. M., & Elsener, K. 1988, Phys. Rev. A, 38, 4395
Baltz, E., & Gondolo, P. 2001, Phys. Rev. Lett., 86, 5004
Baltz, E. A., & Edsjö, J. 1999, Phys. Rev. D, 59, 3511
Barkas, W. H., Dyer, J. N., & Heckman, H. H. 1963, Phys. Rev. Lett., 11, 26
Battiston, R. 1998a, Nucl. Phys. B (Proc. Suppl.), 65, 19
———. 1998b, in Dark Matter: Proceedings of DM97, 1st Italian Conference on Dark Matter, ed. P. Salucci (Florence: Studio Editoriale Fiorentino), 39
Beck, W. A., Wilets, L., & Alberg, M. A. 1993, Phys. Rev. A, 48, 2779
Belotsky, K. M., Golubkov, Y. A., Khlopov, M. Y., Konoplich, R. V., & Sakharov, A. S. 2000, Physics of Atomic Nuclei, 63, 233

Berger, M. J., Coursey, J. S., & Zucker, M. A. 1999, ESTAR, PSTAR, and ASTAR: Computer Programs for Calculating Stopping-Power and Range Tables for Electrons, Protons, and Helium Ions (Version 1.21; Gaithersburg: NIST)
Bergström, L., Edsjö, J., & Gondolo, P. 1998, Phys. Rev. D, 58, 3519
Bergström, L., Edsjö, J., & Ullio, P. 1999, ApJ, 526, 215
Bergström, L., & Gondolo, P. 1996, Astropart. Phys., 5, 263
Bertin, A., et al. 1996, Phys. Lett. B, 369, 77
Bottino, A., Donato, F., Fornengo, N., & Salati, P. 1998, Phys. Rev. D, 58, 123503
Brown, H. N., et al. 2001, Phys. Rev. Lett., 86, 2227
Brückner, W., et al. 1990, Z. Phys. A, 335, 217
Cohen, J. S. 2000, Phys. Rev. A, 62, 2512
Day, T. B., Snow, G. A., & Sucher, J. 1959, Phys. Rev. Lett., 3, 61
Donato, F., Fornengo, N., & Salati, P. 2000, Phys. Rev. D, 62, 043003
Donato, F., Maurin, D., Salati, P., Barrau, A., Boudoul, G., & Taillet, R. 2001, ApJ, 563, 172
Edsjö, J. 1997, Ph.D. thesis, Uppsala Univ. (hep-ph/9704384)

Edsjö, J., & Gondolo, P. 1997, Phys. Rev. D, 56, 1879
Ferrell, R. 1960, Phys. Rev. Lett., 4, 425
Gondolo, P. 2001, in Neutrino 2000: Proceedings of the XIXth International Conference on Neutrino Physics and Astrophysics, ed. J. Law, R. W. Ollerhead, & J. J. Simpson (New York: Elsevier)
Harrison, F. A., et al. 2001, Nucl. Instrum. Methods Phys. Res. A, in press
Hartmann, F. J. 1990, Electromagnetic Cascade and Chemistry of Exotic Atoms, ed. L. M. Simons, D. Horváth, & G. Torelli (New York: Plenum), 127
Hayano, R. S., et al. 1994, Phys. Rev. Lett., 73, 1485
Hubbell, J. H., & Seltzer, S. M. 1997, Tables of X-Ray Mass Attenuation Coefficients and Mass Energy-Absorption Coefficients (Version 1.02; Gaithersburg: NIST)
Jacot-Guillarmod, R., Bienz, F., Boschung, M., Piller, C., Schaller, L. A., Schellenberg, L., Schneuwly, H., & Siradovic, D. 1988, Phys. Rev. A, 37, 3795
Jungman, G., & Kamionkowski, M. 1994, Phys. Rev. D., 49, 2316

Jungman, G., Kamionkowski, M., & Griest, K. 1996, Phys. Rep., 267, 195
Keck, J. W., et al. 2001, ApJ, 563, 172
Kurki-Suonio, H., & Sihvola, E. 2000, Phys. Rev. Lett., 84, 3756
Leo, W. R., & Haase, D. G. 1994, Techniques for Nuclear and Particle Physics Experiments (2d rev. ed.; Berlin: Springer)
MacGibbon, J. H., & Carr, B. J. 1991, ApJ, 371, 447
Maki, K., Mitsui, T., & Orito, S. 1996, Phys. Rev. Lett., 76, 3474
Mandic, V., Baltz, E., & Gondolo, P. 2001, Phys. Rev. D, submitted
Nakamura, S. N., et al. 1994, Phys. Rev. A, 49, 4457
Reifenröther, G., & Klempt, E. 1989, Nucl. Phys. A, 503, 885
Ryufuku, H., Sasaki, K., & Watanabe, T. 1980, Phys. Rev. A., 21, 745
Saeki, T., et al. 1998, Phys. Lett. B, 422, 319
Simon, M., Molnar, A., & Roesler, S. 1998, ApJ, 499, 250
Streitmatter, R. E. 1996, Nuovo Cimento, 19, 835
Wells, J. D., Moiseev, A., & Ormes, J. F. 1999, ApJ, 518, 570
Zombeck, M. V. 1982, Handbook of Space Astronomy and Astrophysics (Cambridge: Cambridge Univ. Press)